RESEARCH PAPER

Rapid and Simple synthesis of TiO_2 and Titanium Dioxide-Nickel Ferrite Nanocomposite Applying Lemon Extract as a Green Capping Agent and the Study of Their Photocatalytic Behavior

Mostafa Soltani [1], **Farnaz Maghazeii** [2] *

[1] Master of Science Student in Nano Physics, Ar.C. , Islamic Azad University, Arak, Iran

[2] Mathematics & Physics Department, Ar.C. , Islamic Azad University, Arak, Iran

ARTICLE INFO

Article History:
Received 05 February 2025
Accepted 27 January 2026
Published 01 April 2026

Keywords:
Magnetic nanoparticles
Nanocomposite
Photocatalytic behavior
Toxic dyes

ABSTRACT

In this research, we used a fast and simple method for synthesis of titanium dioxide (TiO_2) and nickel ferrite ($NiFe_2O_4$) nanostructures: microwave assisted co-precipitation method using water solvent applying lemon extract as a green capping agent in the solvent and again without it. Titanium dioxide/nickel ferrite ($TiO_2/NiFe_2O_4$) nanocomposite was prepared by the same method. The morphology and particles size of samples were studied by scanning electron microscopy (SEM). The porous nanostructure of $TiO_2/NiFe_2O_4$ were ideal for photocatalytic behavior. The crystallographic properties of products were analyzed using X-ray diffraction technique. The magnetic property of $NiFe_2O_4$ and $TiO_2/NiFe_2O_4$ nanoparticles was determined by vibrating sample magnetometry (VSM). Both products had soft ferromagnetic properties. The photocatalytic behavior of TiO_2 and prepared nanocomposite was studied by measuring degradation efficiency of two different acidic dyes irradiated under UV-visible light at different irradiation times. The results confirmed that both products have photocatalytic properties, but the nanocomposite has a higher photocatalytic activity due to coupling of two semiconductors, which can be employed for effective charge separation and increase of lifetime in the charge carriers.

How to cite this article
Soltani M., Maghazeii F. Rapid and Simple synthesis of TiO_2 and Titanium Dioxide-Nickel Ferrite Nanocomposite Applying Lemon Extract as a Green Capping Agent and the Study of Their Photocatalytic Behavior. J Nanostruct, 2026; 16(2):2276-2287. DOI: 10.22052/JNS.2026.02.072

INTRODUCTION

Magnetism is a phenomenon by which materials exert an attractive or repulsive force on other similar magnetic materials. The origin of the magnetic properties of the material is attributed to the moving electrons of the material and the magnetic field is not a central field. That is, there is no magnetic unipolarity. All materials that are magnetized by applying a magnetic field are called magnetic materials. The origin of magnetization in atoms is the amount of orbital angular motion and the amount of spin motion of electrons. These two types of electron movement produce a magnetic field, but determining the relative magnetic

* Corresponding Author Email: Fa.Maghazeii@iau.ac.ir

orientation of electrons located in an ion placed in a crystal lattice depends on the interaction between electrons. The microscopic cause of the magnetic properties is the half-filled orbitals in the elements. However, some elements, although they have half-filled orbitals, are not considered as magnetic materials because they form covalent bonds with other atoms of their type when they exist in nature [1-5].

Nickel ferrite has an inverted spinel structure in which the tetrahedral sites (A) average Fe^{2+} and Ni^{2+} ions are occupied. The cubic unit cell consists of 56 atoms, 32 ions Oxygen, which are distributed in a closed cubic structure, and 24 cations, which occupy 8 of 64 positions. Tetrahedral (A position) and 16 positions out of 32 octahedral positions are occupied. Nickel ferrite is the most suitable material for device applications in the wavelength range above microwave and lower than mm. $NiFe_2O_4$ is a soft magnetic material which has many advantages such as: abundant source, low price, high electrical resistance, low dissipation, chemical stability, excellent mechanical hardness, low coercivity and balanced saturation magnetization. These advantages have made nickel ferrite to have many industrial applications such as high density magnetic recording, magnetic fluxes, high Frequency devices and photocatalyst industry [6-10].

During the last decade, the photochemistry of nanoscale semiconductor particles, as one of research fields have been growing rapidly. This interest is due to the characteristics of photophysical and photocatalytic nanoscale particles that have unique optical and electrical properties, quantum effect, compact size compared to bulk material. In addition, nanoparticles show high adsorption capability in both liquid and gas phases. By reducing the size of the particles to the nano scale, the number of atoms in the surface is increased and causes an increase in the ratio of surface to volume. With this access, more active sites are created and the transfer rate of cargo carriers increases. In fact, due to the increase of surface atoms numbers, the more charge carriers can participate in the photocatalytic activity and the speed of photocatalytic activity increases significantly . These reasons have made nanomaterials suitable for photocatalytic applications [11-16].

Metal oxides have long been used as photocatalysts. Duo to distinct band gap, these oxides have the ability to absorb both visible and UV light photons [11]. TiO_2 particularly in anatase phase with E_g=3.2 eV seems to be one of the most usable semiconductor metal oxides for photocatalytic applications because of its chemical stability, non toxicity, water insolubility, higher oxidizing capacity and of course low cost [17-20]. However TiO_2 has two major problems: high recombination rate between e^- - h^+ pairs which results a low photocatalytic efficiency and large band gap that is limited photocatalytic activity to the UV region only [15,21-24].

Due to small size of nanoparticles, separating photocatalytic reaction products from the aqueous medium is too difficult. Magnetic particles can solves this problem in the presence of external magnetic field [25-27]. Soft magnetic materials like spinel ferrites are one of the main options because of their thermal and chemical stabilities and desired magnetic properties [28-32]. Ferrites also help to improve the photocatalytic activity [33-35].

In this research, at first we synthesized nickel ferrite and titanium dioxide nanoparticles using an easy method: microwave assisted co-precipitation method applying lemon extract as a green capping agent in the solvent and again without it. In second step, $TiO_2/NiFe_2O_4$ core-shell magnetic nanocomposite was prepared using the same method. XRD, SEM and VSM analysis for the samples were done. Finally, the photocatalytic behavior of synthetic nanocomposite for degradation of methyl orange and acid brown toxic dyes via UV-visible light irradiation was studied.

MATERIALS AND METHODS

Materials and devices

We used $NiSO_4.6H_2O$, $Fe(NO_3)_3.9H_2O$, $Ti\{OCH(CH_3)_2\}_4$, NaOH and ammonia from Merck company and double distilled water, hydrochloric acid and ethanol as raw materials for preparing of our nanomaterials. The simple kitchen microwave oven from Panasonic Company with power of 600 Watt was used for heating and the time measured by standard chronometer. To determine the structural characterization of samples, we used XRD analysis with CuK_α (λ= 1.5418Å) in the range of 2θ= 10°- 90°. The SEM images were obtained by MIRA3 TESCAN SEM. Magnetic properties were evaluated using a VSM at room temperature (Magnetic Daghigh Daneshpajouh Co., Iran) in an applied magnetic field sweeping between

±10000Oe.

Synthesis of nickel ferrite via microwave assisted co-precipitation method

For the synthesis of nickel ferrite nanoparticles, 0/5 g of nickel sulfate hexahydrate ($NiSO_4.6H_2O$, molecular weight: 262.85 g/mole) with 1/39 g of iron nitrate ninehydrate ($Fe(NO_3)_3.9H_2O$, molecular weight: 414.1 g/mole) with a molar ratio of 1:2 were dissolved in 200 ml double distilled water and was stirred by a magnetic stirrer. As a green capping agent, 10 ml of lemon extract were added to the solution. After achieving a homogeneous and clear solution, the solution was placed in the center of the microwave oven and NaOH solution (1M) was added drop by drop to the solution under microwave radiations with the power of 600 Watt for 7 min. (20s on and 1min off). pH of solution was adjusted at 11 which measured by calibrated pH meter. Then we centrifuged obtained precipitates and washed them thrice with deionized water. The resulting sediment dried in oven at 40°C for 24 hours and calcinated at 600°C for 2 hours. The synthesis was repeated once without using lemon extract in the solvent.

Synthesis of titanium dioxide with microwave method

1 g of titanium isopropoxide ($Ti\{OCH(CH_3)_2\}_4$) was dissolved in 10 ml of 99.9% absolute ethanol and placed on a stirrer for 30 minutes. The produced solution was then placed in the microwave and heated at 600 Watt for 10 minutes (alternating 20 seconds heating and turning off for one minute). When the apparatus was switched off, about 10 ml of ammonia(2M) was gradually added to the solution as a precipitator until the pH reached 11. After 2 hours for cooling down, the formed sediment matrix was centrifuged two times at different speeds and washed with deionized water and then placed in oven at 40°C for 24 hours for drying.

Preparation of $TiO_2/NiFe_2O_4$ core-shell nanocomposite

To prepare $TiO_2/NiFe_2O_4$ nanocomposite, it is sufficient to synthesize titanium dioxide in the presence of nickel ferrite nanoparticles. For this purpose, 1 g of synthesized nickel ferrite is well pounded in a mortar and poured into a solution of 1 g of titanium isopropoxide ($Ti\{OCH(CH_3)_2\}_4$) in 15 ml of ethanol (molar ratio: 1:1). The prepared solution was stirred at room temperature for 5 hours until the nickel ferrite particles are well dispersed in the solution.

The solution was then put in the ultrasonic device with a power of 50% and 400 watts at room temperature for 30 min. to aid dispersion. Then the solution was placed in the microwave and the steps of heating, sedimentation, centrifugation

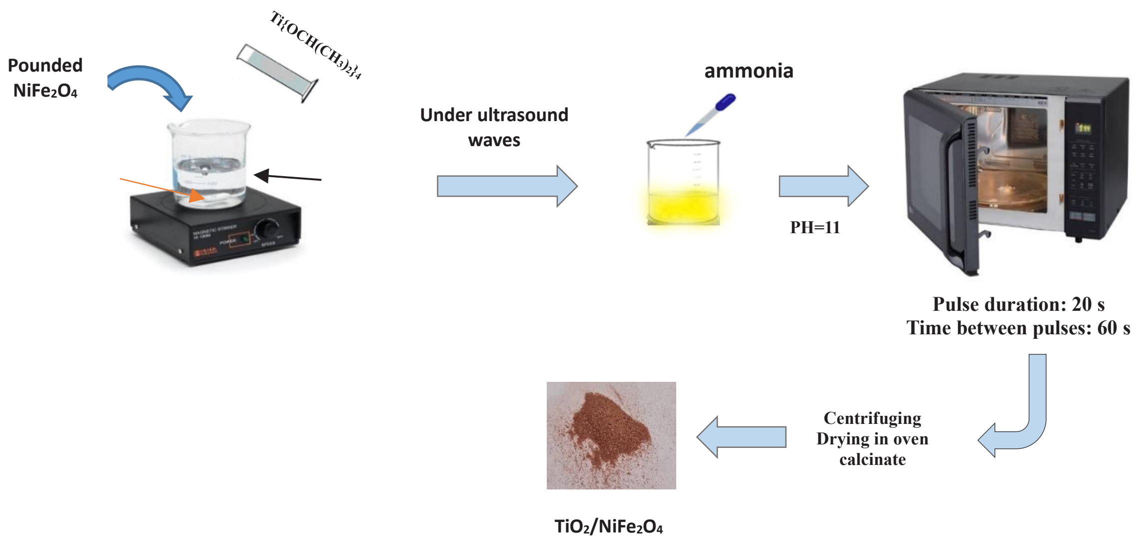

Fig. 1. Schematic diagram for $TiO_2/NiFe_2O_4$ nanocomposite synthesis.

and drying were repeated exactly as mentioned in sec. 2.2. Titanium dioxide covered the nickel ferrite like a layer and the core-shell $TiO_2/NiFe_2O_4$ nanocomposite was formed. Fig. 1 schematically shows the synthesis of this nanocomposite.

RESULTS AND DISCUSSION

XRD analysis results

Fig. 2 indicates the x-ray diffraction (XRD) patterns of $NiFe_2O_4$ nanoparticles. The pattern reveals the typical diffraction pattern of pure cubic

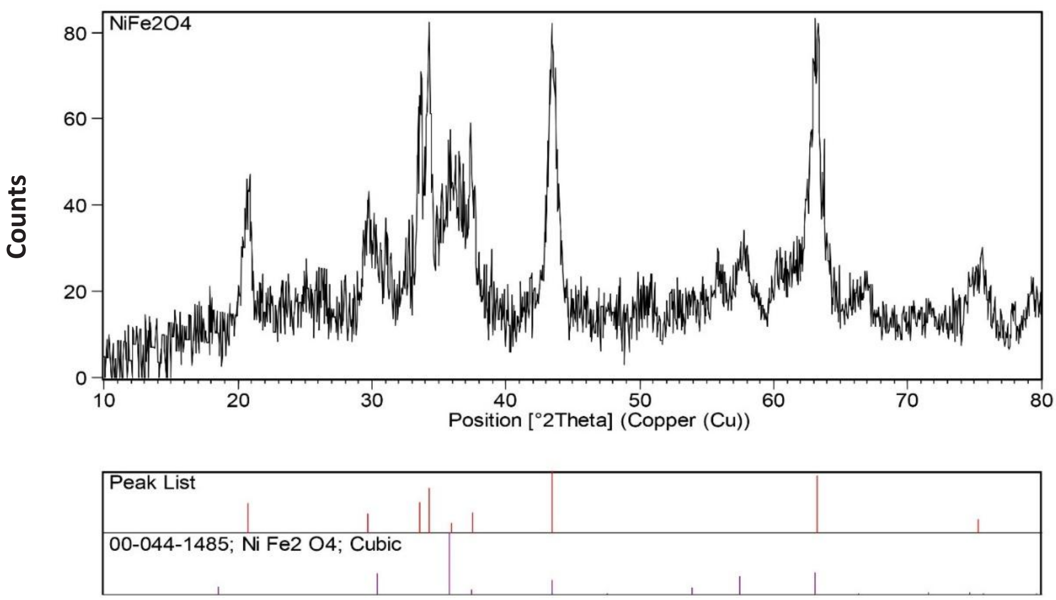

Fig. 2. XRD pattern of nickel ferrite nanoparticles.

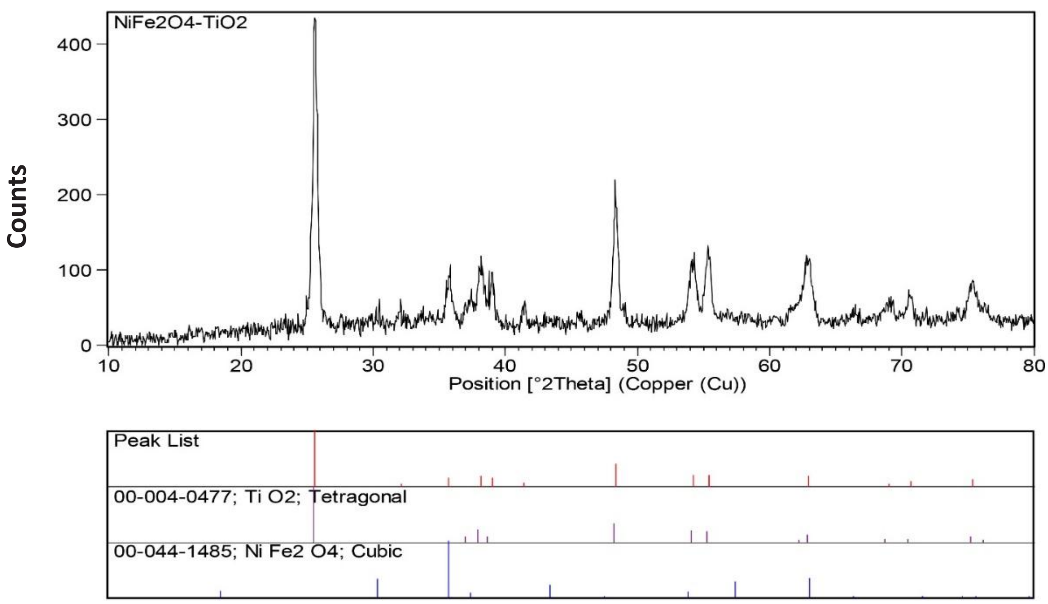

Fig. 3. XRD pattern of TiO_2/ $NiFe_2O_4$ nanocomposite.

phase. There are two sharp and large peaks in 2θ= 43.4° and 2θ= 63.2° and two smaller peaks in 2θ= 37.4° and 2θ= 57.9° in agreement with pure phase of $NiFe_2O_4$ (JCPDS 00-044-1458). Some peaks extremely close together and sometimes even forming one peak with two tips suggests the fact that the sample has been thermally crystallized and the cool down after the thermal treatment happens in a very rapid pace (quanching process).

Also, the XRD pattern of TiO_2/ $NiFe_2O_4$ nanocomposite is seen in the Fig. 3. The presence of several sharp peaks matching the TiO_2 pattern (JCPDS 00-004-0477) with tetragonal structure and two smaller peaks in 2θ= 37.4° and 2θ= 63.2° matching the peaks of $NiFe_2O_4$ XRD pattern indicates that the nanocomposite has been formed.

The crystallite size of samples was calculated from the full width at half maximum (FWHM) of the diffraction peaks using Debye-Scherrer's equation:

$$D = k\lambda/\beta\cos\theta \quad (1)$$

where d is the average crystalline dimension perpendicular to the reflecting phases, λ is the x-ray wavelength, k is Scherrer constant (0.94), β is the FWHM intensity of a Bragg reflection excluding instrumental broadening and θ is the Bragg angle [36,37]. Table 1 indicates the calculated average crystallite size of the both samples.

SEM analysis of samples

Fig. 4a and b illustrate SEM images of nickel ferrite samples synthesized by microwave assisted co-precipitation method without and with lemon

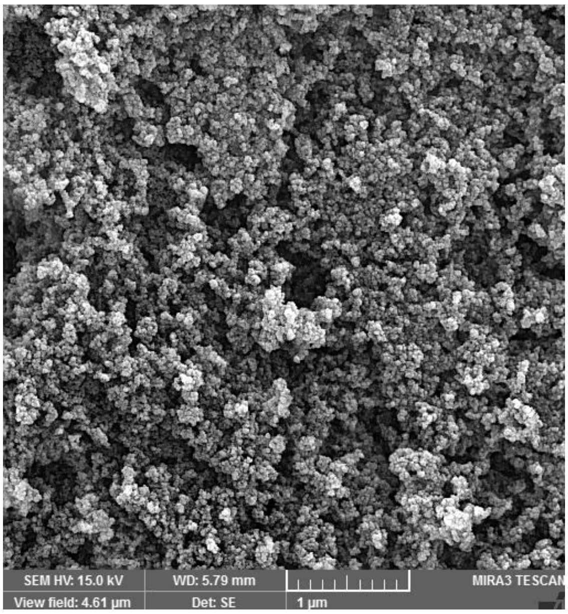

(a)

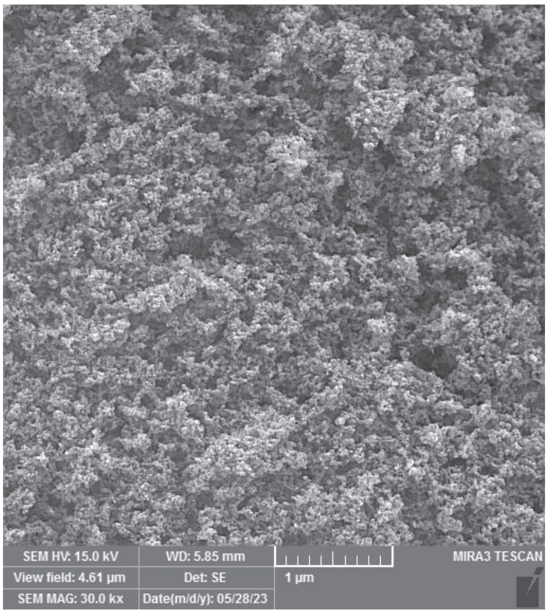

(b)

Fig. 4. The SEM images of nickel ferrite synthesized by microwave assisted co-precipitation method: a) without lemon extract b) with lemon extract in the solvent.

Table 1. Average crystallite size of the samples.

Sample	d (nm)
$NiFe_2O_4$	57
$TiO_2/NiFe_2O_4$	66

extract in the solvent, respectively. By comparing images of (4a) and (4b), we can see that by adding lemon extract to the solvent, a more uniform nanostructure with smaller grains and almost without agglomeration was obtained, as we know lemon extract has citric acid in its structure. The average size of nanoparticles for nickel ferrite samples with and without lemon extract were achieved from SEM images 75 and 63 nm, respectively.

SEM image of titanium dioxide synthesized by microwave method without lemon extract in its solvent has been shown in in Fig. 5. Small and uniform grains with a little agglomeration can be seen. The average size of 70 nm was achieved for TiO_2 nanoparticles. The porous structure which is one of the characteristics of a good absorbent, is not seen in the image therefore, it is expected that this sample does not have an ideal photocatalytic behavior.

Fig. 6a, and b illustrates SEM images of titanium dioxide-nickel ferrite nanocomposite prepared under microwave irradiation without and with lemon extract in the solvent, respectively.

The porous structure in both images indicates the readiness of a suitable nanostructure of

nanocomposite for photocatalytic behavior but, agglomeration of island-shaped grains with small voids between them are seen in SEM image of Fig. 6-a. By adding lemon extract to the solvent, the improvement of the composite nanostructure and the reduction of island-shaped grains can be seen in the Fig. 6-b. As mentioned earlier, the citric acid in lemon extract has resulted in a more uniform structure with smaller grains.

As we expected, nanoparticles in our composite were bigger than the particles in each of the components individually. The average sizes of nanoparticles in the composite were 82 nm in the absence of lemon extract in the solvent and 78 nm in the presence of it in the solvent.

Fig. 7 reveals the average particle diameters for all synthesized samples that compared through a bar chart.

Magnetic properties of $NiFe_2O_4$ and $TiO_2/NiFe_2O_4$ nanocomposite

Magnetic properties of $CuFe_2O_4$ and our nanocomposite were studied by VSM instrument at room temperature. Fig. 8a, and b shows the hysteresis loops of these samples. The curve in Fig. 8a indicates nickel ferrite exhibit soft ferromagnetic behavior with a large enough magnetization which make it suitable for the core of a photocatalyst. Also, the hysteresis loop related to the $TiO_2/NiFe_2O_4$ nanocomposite shown in Fig. 8b reveals that this sample has also ferromagnetic properties but with lower saturation and residual

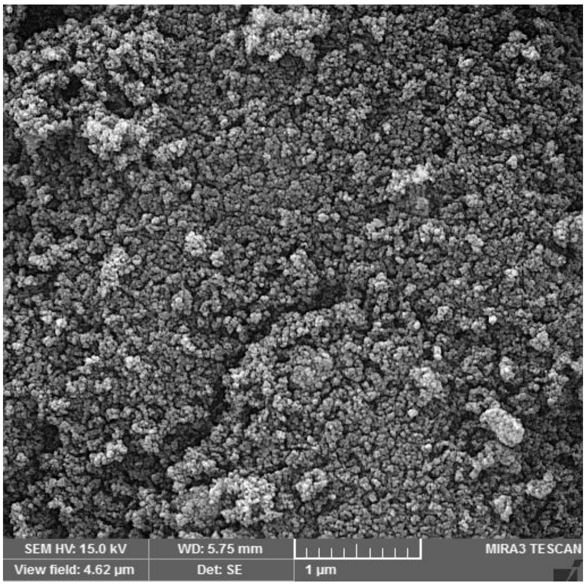

Fig. 5. SEM image of titanium dioxide prepared under microwave irradiation without lemon extract.

magnetization than $NiFe_2O_4$. Table 2 shows magnetic parameters related to these two samples.

Photocatalytic activity of TiO_2 and TiO_2/$NiFe_2O_4$ nanocomposite

The photocatalytic activity of titanium

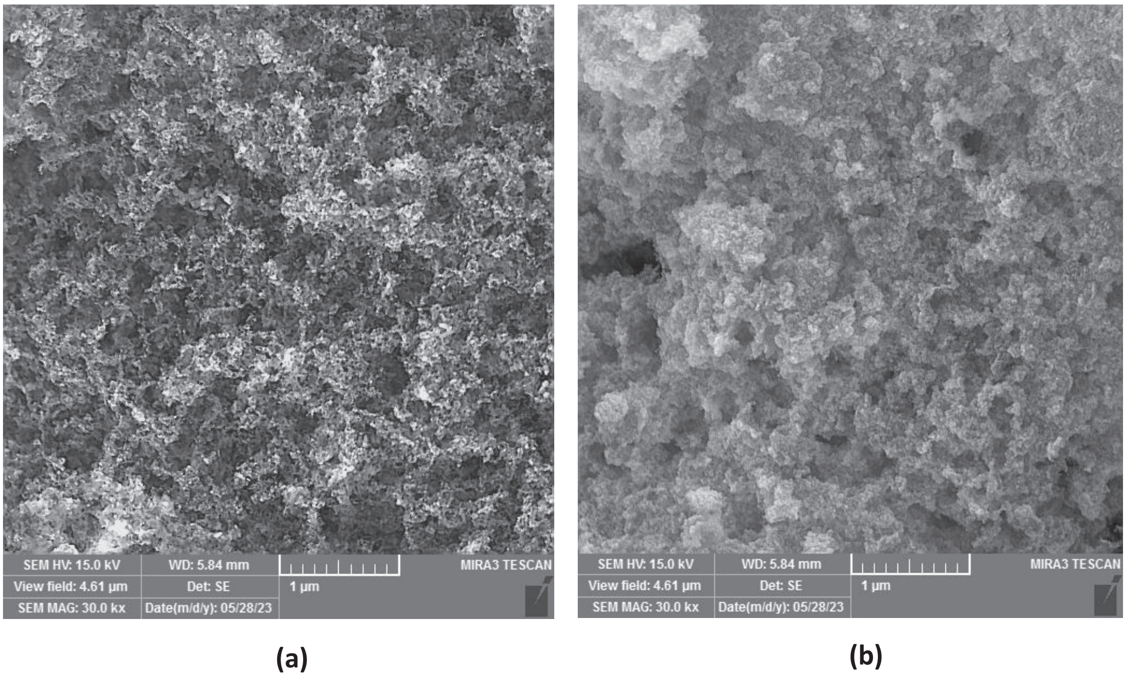

Fig. 6. The SEM images of TiO_2/$NiFe_2O_4$ nanocomposite prepared by microwave assisted co-precipitation method: a) without lemon extract b) with lemon extract in the solvent.

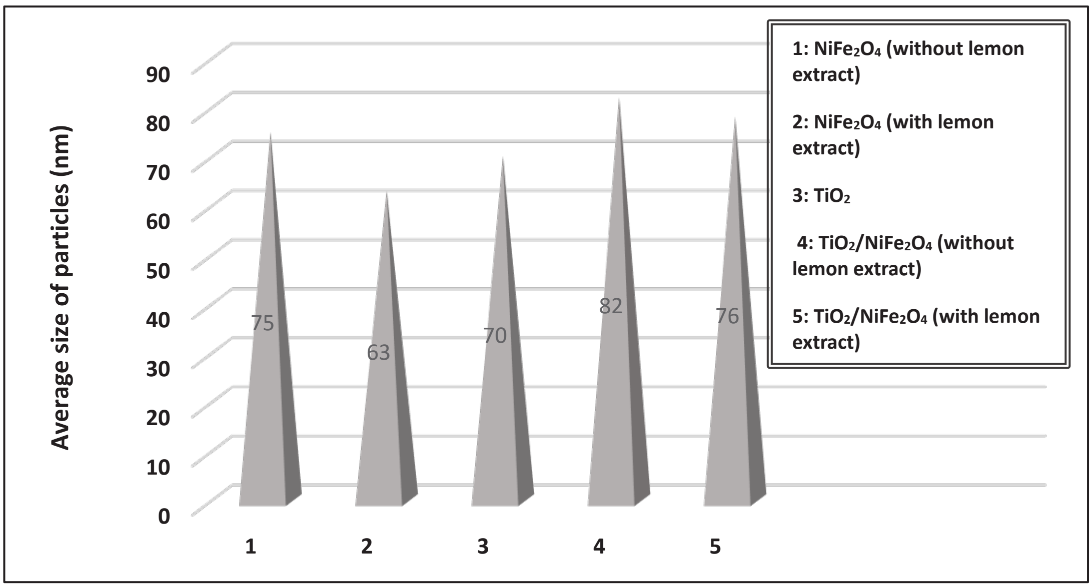

Fig. 7. The average size of particles for all synthesized samples.

dioxide and titanium dioxide/nickel ferrite were investigated in this work.

Active radicals that generated by these materials react with organic pollutants, deleted them and produce CO_2 and H_2O.

Titanium dioxide with $E_g = 3.2$ eV is activated with UV light. The electrons are excited by absorbing UV light from valence band to conduction band. The electron- hole pairs are able to reduce and/or oxidize a molecule adsorbed (O_2, H_2O and etc.) on the photocatalyst semiconductor surface and produce hydroxyl radicals ($OH^·$) and superoxide anion radicals ($O_2^{·-}$). Following reactions are happened during degradation of pollutants on the TiO_2 surface:

$$TiO_3 + hv\ (\text{UV light}) \rightarrow e^- + h^+ \quad (2)$$

$$H_2O + h^+ \rightarrow OH^· + H^+ \quad (3)$$

$$O_2 + 2e^- + 2H^+ \rightarrow H_2O_2 \quad (4)$$

$$H_2O_2 + e^- + H^+ \rightarrow OH^· + H_2O \quad (5)$$

$$2H_2O + 2h^+ \rightarrow 2H^+ + H_2O_2 \quad (6)$$

Addition of nickel ferrite (with $E_g = 1.54$ eV in the region of visible light energy) to TiO_2 and preparation of $TiO_2/NiFe_2O_4$ nanocomposite, in addition to helping to remove photocatalytic reaction products from the aqueous medium by applying an external magnetic field, also helps to improve the photocatalytic properties of titanium dioxide.

In $TiO_2/NiFe_2O_4$ nanocomposite, the transfer of holes and electrons occurs for both materials (Increasing charge carriers and as a result, increase the photocatalytic reactions). It is expressive of reduced recombination of charge carriers, leading to availability of more reactive radicals in nanocomposite for the enhanced photocatalytic activity. Superoxide anion radicals generated by $NiFe_2O_4$ can react with hydrogen peroxide and leading to hydroxyl radical's production [38,39]:

$$H_2O_2 + O_2^{·-} \rightarrow OH^· + OH^- + O_2 \quad (7)$$

Fig. 9a and b shows the mechanism of photocatalytic activity for TiO_2 semiconductor and the coupling mechanism of two materials for this activity in $TiO_2/NiFe_2O_4$ nanocomposite,

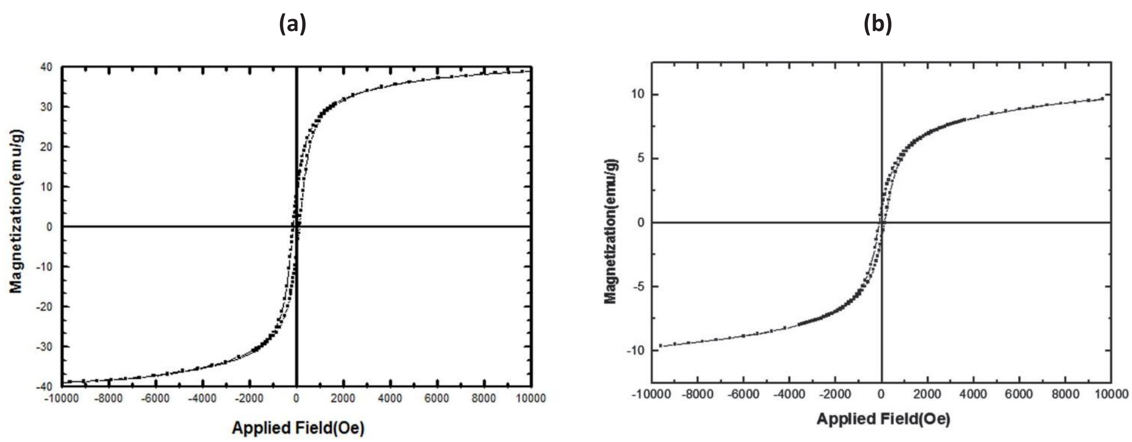

Fig. 8. Hysteresis loop for: a) $NiFe_2O_4$ b) $TiO_2/NiFe_2O_4$ nanocomposite.

Table 2. Magnetic parameters of $NiFe_2O_4$ nanoparticles and $TiO_2/NiFe_2O_4$ nanocomposite.

Sample	Saturation magnetization (M_s) (emu/g)	Residual magnetization (M_r) (emu/g)	Coercivity (Oe)	$\frac{M_r}{M_s}$
$NiFe_2O_4$	39	8	90	0.205
TiO_2/NiFe2O4	9.6	2.8	50	0.291

respectively [40].

To analyze the photocatalytic behavior of prepared nanocomposites, we used methyl orange ($S_3NaO_3N_{14}H_{14}C$) and acid brown ($C30H20N8Na_2O_{13}S_2$) as natural contaminant. These dyes are widely used in photocatalytic researches due to their structural stability.

First, using distilled water as solvent, color solutions were prepared with concentration of 100ppm of these two dyes and for obtaining of acidic dye solutions, hydrochloric acid were added to them until their pH reached 4. Then the absorption spectra of these solutions under UV-visible radiation in the wavelength range of 200-700nm were obtained by UV-visible spectrometer and the maximum absorption wavelength (λ_{max}) was determined for each dye solution.

In the next step, 20 ml of dye solutions were poured in two separate container and 0.1 g of TiO_2 and TiO_2 /$NiFe_2O_4$ nanocomposite were separately added to them as adsorbent. After resting in a dark place for a few hours, the dye solutions were stirred with a magnetic stirrer. They were exposed to UV-visible radiation for 30 minutes. This experiment was repeated for 60 and 120 min. irradiation time with the same conditions. At the end of the irradiation time for each of the dye solutions, the final absorbance

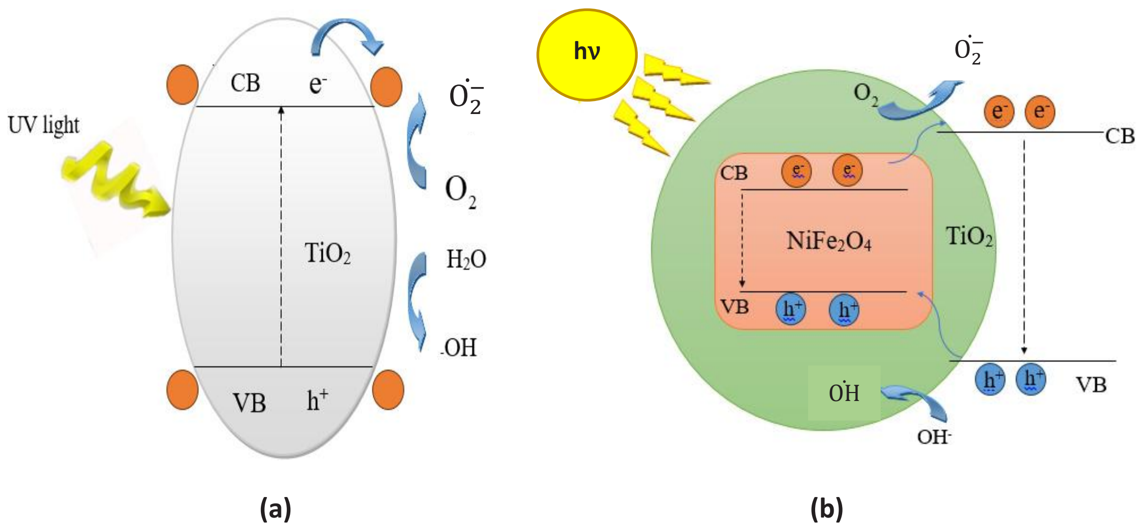

Fig. 9. The mechanism of photocatalytic activity for: a) TiO_2 semiconductor b) $TiO_2/NiFe_2O_4$ nanocomposite.

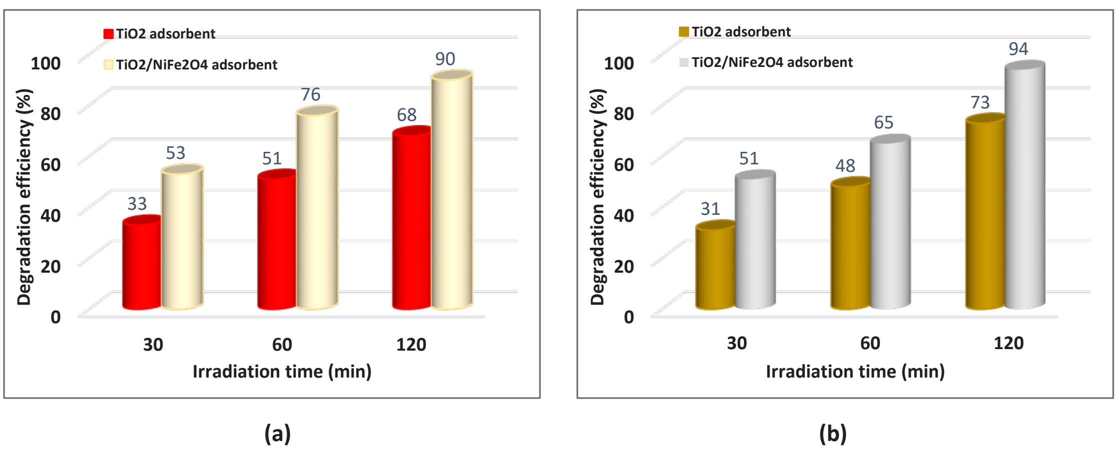

Fig. 10. The results of degradation efficiency for dye solutions with two different adsorbents at different irradiation times: a) methyl orange b) acid brown.

at λ_{max} was determined by the spectrometer and using these results, the percentage of reduction of the dye concentration (degradation efficiency) was obtained from the following equation in each experiment:

$$\eta = (C_0 - C_f)/C_0 \times 100 \quad (8)$$

Where C_0 and C_f are the initial and final azo dye concentrations respectively.

Fig. 10a and b visualize the results of degradation efficiency for two 100 ppm dye solutions contain TiO_2 and $TiO_2/NiFe_2O_4$ as two different adsorbents at different irradiation times. Degradation efficiency increases with the irradiation time for both adsorbents but as expected, the prepared nanocomposite exhibited more photocatalytic activity than TiO_2 because of coupling of two materials. With prolongation of irradiation time, the amount of reactive free radicals will increase.

Fig. 11a and b illustrates the changes in the dye concentration by adding 0.1 g of TiO_2 and $TiO_2/NiFe_2O_4$ nanocomposite to 20 ml of both different dye solutions with 100ppm concentration of

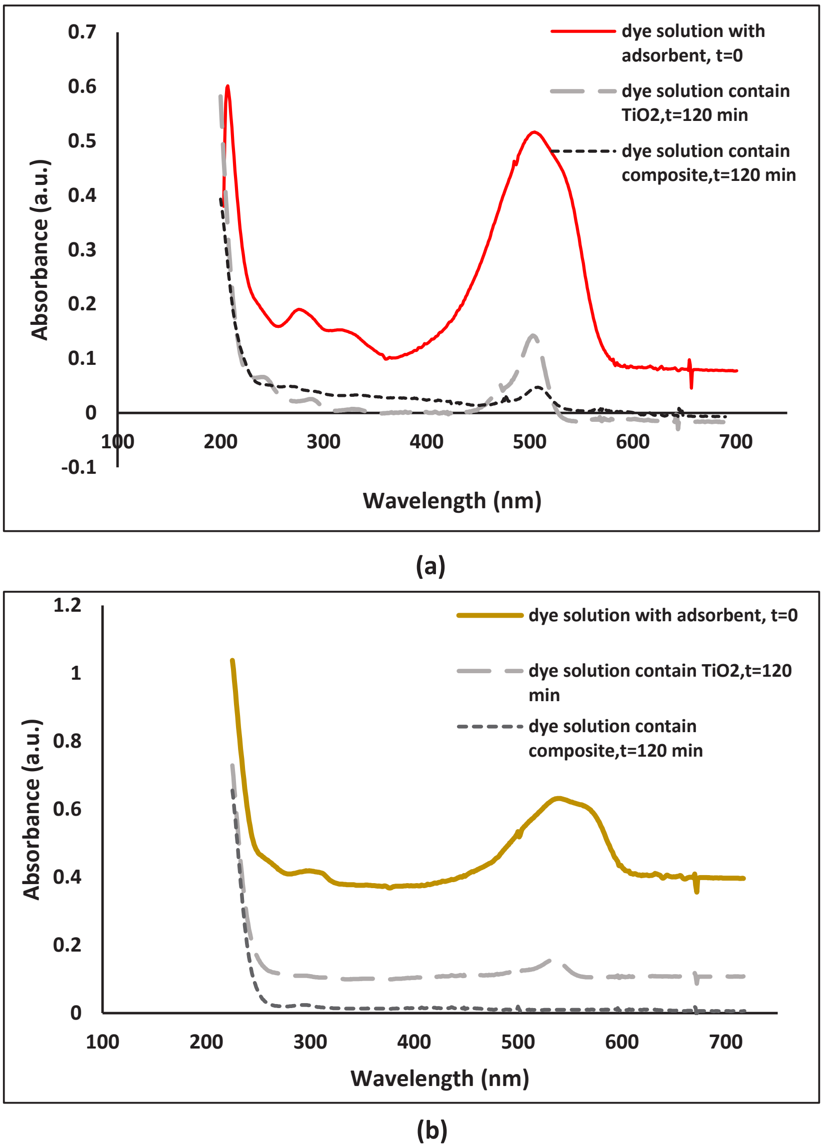

Fig. 11. The effect of adsorbents on degradation of dye solutions under 120 min irradiation: a) methyl orange b) acid brown.

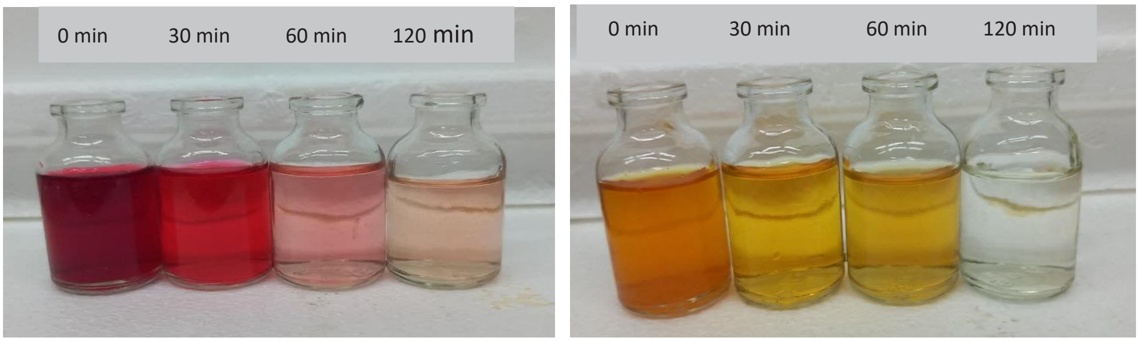

(a) (b)

Fig. 12. Photo degradation of 20 ml of azo dyes with 0.1 g $TiO_2/NiFe_2O_4$ adsorbent and 100 ppm dye concentration under 0, 30, 60 and 120 min solar irradiation: a) methyl orange b) acid brown.

dye after 120 minutes irradiation from UV-vis absorption spectra. Also Fig. 12 a and b shows the color degradation of these dye solutions contain $TiO_2/NiFe_2O_4$ nanocomposite during the irradiation time.

CONCLUSION

In this study, $NiFe_2O_4$ and TiO_2 nanoparticles and $TiO_2/NiFe_2O_4$ nanocomposite were synthesized by microwave assisted co-precipitation method applying lemon extract as a green capping agent in the solvent and again without it. By addition of lemon extract to the solvents, the nanostructure of the samples was improved and grains size of the samples became smaller.

The hysteresis curves obtained using the VSM analysis showed that both of $NiFe_2O_4$ and $TiO_2/NiFe_2O_4$ were soft ferromagnetic materials. Finally, the photocatalytic behavior of TiO_2 and $TiO_2/NiFe_2O_4$ nanocomposite was studied using the degradation of methyl orange and acid brown dye solutions with 100ppm dye concentration under different times of UV-visible light irradiation. Both adsorbents had the photocatalytic properties but, the prepared nanocomposite exhibited more photocatalytic activity than TiO_2 semicondutor. The color degradation increased with increasing the irradiation time until the degradation efficiency reached almost 90% for both dye solutions after 120 minutes of irradiation with $TiO_2/NiFe_2O_4$ as adsorbent.

CONFLICT OF INTEREST

The authors declare that there is no conflict of interests regarding the publication of this manuscript.

REFERENCES

1. Saffarzadeh S, Nabiyouni G, Ghanbari D. Preparation of $Ni(OH)_2$, NiO and $NiFe_2O_4$ nanoparticles: magnetic and photo-catalyst $NiFe_2O_4$–NiO nanocomposites. Journal of Materials Science: Materials in Electronics. 2016;27(12):13338-13350.
2. Kinemuchi Y, Ishizaka K, Suematsu H, Jiang W, Yatsui K. Magnetic properties of nanosize $NiFe_2O_4$ particles synthesized by pulsed wire discharge. Thin Solid Films. 2002;407(1-2):109-113.
3. Houlding TK, Gao P, Degirmenci V, Tchabanenko K, Rebrov EV. Mechanochemical synthesis of $TiO_2/NiFe_2O_4$ magnetic catalysts for operation under RF field. Materials Science and Engineering: B. 2015;193:175-180.
4. Nasseh N, Barikbin B, Taghavi L, Nasseri MA. Adsorption of metronidazole antibiotic using a new magnetic nanocomposite from simulated wastewater (isotherm, kinetic and thermodynamic studies). Composites Part B: Engineering. 2019;159:146-156.
5. Ahmadi A, Ghanbari D, Nabiyouni G. Facile synthesis of hexagonal strontium ferrite nanostructures and hard magnetic poly carbonate nanocomposite. nano Online: De Gruyter; 2018.
6. Hosseini M, Rezaei Ashtiani H, Ghanbari D. Properties Investigation of Surface Nanocomposites Fabricated by Friction Stir Processing and Magnetic Ferrite Nanoparticles. Transactions of the Indian Institute of Metals. 2022;75(7):1885-1898.
7. Gharagozlou M. Study on the influence of annealing temperature and ferrite content on the structural and magnetic properties of $x(NiFe_2O_4)/(100-x)SiO_2$ nanocomposites. J Alloys Compd. 2010;495(1):217-223.
8. Mitra S, Mandal K, Anil Kumar P. Temperature dependence of magnetic properties of NiFe2O4 nanoparticles embeded in SiO_2 matrix. J Magn Magn Mater. 2006;306(2):254-259.
9. Liu Y, Cherkasov N, Gao P, Fernández J, Lees MR, Rebrov EV. The enhancement of direct amide synthesis reaction rate over TiO_2 @SiO_2 @$NiFe_2O_4$ magnetic catalysts in the continuous flow under radiofrequency heating. J Catal. 2017;355:120-130.
10. Saffarzadeh S, Nabiyouni G, Heidary F. A short time microwave method for synthesis of magnetic $NiFe_2O_4$/NiO nanocomposites as a clean technology in photocatalytic degradation of water pollutants. Journal of Materials Science: Materials in Electronics. 2019;30(9):8171-8181.
11. Kaur A, Umar A, Anderson WA, Kansal SK. Facile synthesis of CdS/TiO_2 nanocomposite and their catalytic activity for ofloxacin degradation under visible illumination. J

Photochem Photobiol A: Chem. 2018;360:34-43.
12. Joulaei M, Hedayati K, Ghanbari D. Investigation of magnetic, mechanical and flame retardant properties of polymeric nanocomposites: Green synthesis of MgFe2O4 by lime and orange extracts. Composites Part B: Engineering. 2019;176:107345.
13. Intaphong P, Phuruangrat A, Karthik K, Dumrongrojthanath P, Thongtem T, Thongtem S. Effect of pH on Phase, Morphology and Photocatalytic Properties of BiOBr Synthesized by Hydrothermal Method. Journal of Inorganic and Organometallic Polymers and Materials. 2019;30(3):714-721.
14. Liu X, Dang R, Dong W, Huang X, Tang J, Gao H, et al. A sandwich-like heterostructure of TiO_2 nanosheets with MIL-100(Fe): A platform for efficient visible-light-driven photocatalysis. Applied Catalysis B: Environmental. 2017;209:506-513.
15. Zhu S-R, Wu M-K, Zhao W-N, Yi F-Y, Tao K, Han L. Fabrication of heterostructured $BiOBr/Bi_{24}O_{31}Br_{10}/TiO_2$ photocatalyst by pyrolysis of MOF composite for dye degradation. J Solid State Chem. 2017;255:17-26.
16. Hedayati K, Azarakhsh S, Saffari J, Ghanbari D. Magnetic and Photo-catalyst $CoFe_2O_4$-CdS nanocomposites: Simple preparation of Ni, Co, Zn or Ag-doped CdS nanoparticles. Journal of Materials Science: Materials in Electronics. 2017;28(7):5472-5484.
17. Kudhier MA, Alkareem RASA, Sabry RS. Enhanced photocatalytic activity of TiO_2-CdS composite nanofibers under sunlight irradiation**. Journal of the Mechanical Behavior of Materials. 2021;30(1):213-219.
18. Hardian A, Devikha, Budiman S, Yuliana T, Sujono H, Murniati A, et al. Synthesis of TiO_2-$NiFe_2O_4$ nanocomposites using coprecipitation method as photocatalyst for methylene blue removal. IOP Conference Series: Earth and Environmental Science. 2021;882(1):012022.
19. Sabry RS, Al-Haidarie YK, Kudhier MA. Synthesis and photocatalytic activity of TiO_2 nanoparticles prepared by sol–gel method. J Sol-Gel Sci Technol. 2016;78(2):299-306.
20. Sudhagar S, Kumar SS, Premkumar IJI, Vijayan V, Venkatesh R, Rajkumar S, et al. UV- and visible-light-driven TiO_2/La_2O_3 and TiO_2/Al_2O_3 nanocatalysts: synthesis and enhanced photocatalytic activity. Appl Phys A. 2022;128(4).
21. Li J, Xu X, Liu X, Qin W, Wang M, Pan L. Metal-organic frameworks derived cake-like anatase/rutile mixed phase TiO_2 for highly efficient photocatalysis. J Alloys Compd. 2017;690:640-646.
22. Yousif Q, Haran N. Fabrication of TiO_2 nanotubes via three - electrodes anodization technique under sound waves impact and use in dye-sensitized solar cell. Egyptian Journal of Chemistry. 2020;0(0):
23. Manchwari S, Khatter J, Chauhan RP. Enhanced photocatalytic efficiency of TiO_2/CdS nanocomposites by manipulating CdS suspension on TiO_2 nanoparticles. Inorg Chem Commun. 2022;146:110082.
24. Qutub N, Singh P, Sabir S, Sagadevan S, Oh W-C. Enhanced photocatalytic degradation of Acid Blue dye using CdS/TiO_2 nanocomposite. Sci Rep. 2022;12(1).
25. Lu ZL, Gao PZ, Ma RX, Sun YK, Li DY. Preparation, Characterization and Visible-Light Catalytic Activity of Core-Shell Structure $NiFe_2O_4$; Ferrite Nanoparticles. Key Eng Mater. 2016;680:272-277.
26. Etminan M, Nabiyouni G, Ghanbari D. Preparation of tin ferrite–tin oxide by hydrothermal, precipitation and auto-combustion: photo-catalyst and magnetic nanocomposites for degradation of toxic azo-dyes. Journal of Materials Science: Materials in Electronics. 2017;29(3):1766-1776.
27. Ghanbari D, Sharifi S, Naraghi A, Nabiyouni G. Photo-degradation of azo-dyes by applicable magnetic zeolite Y–Silver–$CoFe_2O_4$ nanocomposites. Journal of Materials Science: Materials in Electronics. 2016;27(5):5315-5323.
28. Kubota M, Kanazawa Y, Nasu K, Moritake S, Kawaji H, Atake T, et al. Effect of heat treatment on magnetic $MgFe_2O_4$ nanoparticles. J Therm Anal Calorim. 2008;92(2):461-463.
29. Chandradass J, Jadhav AH, Kim KH, Kim H. Influence of processing methodology on the structural and magnetic behavior of $MgFe_2O_4$ nanopowders. J Alloys Compd. 2012;517:164-169.
30. Albino M, Fantechi E, Innocenti C, López-Ortega A, Bonanni V, Campo G, et al. Role of Zn^{2+} Substitution on the Magnetic, Hyperthermic, and Relaxometric Properties of Cobalt Ferrite Nanoparticles. The Journal of Physical Chemistry C. 2019;123(10):6148-6157.
31. Hanini A, Kacem K, Gavard J, Abdelmelek H, Ammar S. Ferrite Nanoparticles for Cancer Hyperthermia Therapy. Handbook of Nanomaterials for Industrial Applications: Elsevier; 2018. p. 638-661.
32. Sivakumar N, Gnanakan SRP, Karthikeyan K, Amaresh S, Yoon WS, Park GJ, et al. Nanostructured $MgFe_2O_4$ as anode materials for lithium-ion batteries. J Alloys Compd. 2011;509(25):7038-7041.
33. Xiong C, Chen Q, Lu W, Gao H, Lu W, Gao Z. Novel Fe-based complex oxide catalysts for hydroxylation of phenol. Catal Lett. 2000;69(3-4):231-236.
34. Khojasteh H, Salavati-Niasari M, Mazhari M-P, Hamadanian M. Preparation and characterization of Fe_3O_4@SiO_2@TiO_2@Pd and Fe_3O_4@ SiO_2@ TiO_2@Pd–Ag nanocomposites and their utilization in enhanced degradation systems and rapid magnetic separation. RSC Advances. 2016;6(81):78043-78052.
35. Masoumi S, Nabiyouni G, Ghanbari D. Photo-degradation of azo dyes: photo catalyst and magnetic investigation of $CuFe_2O_4$–TiO_2 nanoparticles and nanocomposites. Journal of Materials Science: Materials in Electronics. 2016;27(9):9962-9975.
36. Devaraja PB, Avadhani DN, Nagabhushana H, Prashantha SC, Sharma SC, Nagabhushana BM, et al. MgO:Dy^{3+} nanophosphor: Self ignition route, characterization and its photoluminescence properties. Mater Charact. 2014;97:27-36.
37. Nowick AS. X-ray diffraction procedures for polycrystalline and amorphous materials. H. P. Klug and L. E. Alexander. John Wiley and Sons, Inc., New York (1954). 716 pages. $15.00. AIChE Journal. 1956;2(1):140-140.
38. Abdi Z, Maghazeii F, Ghanbari D. The Effect of Calcium Perovskite and Newly Developed Magnetic $CaFe_2O_4/CaTiO_3$ Perovskite Nanocomposite on Degradation of Toxic Dyes Under UV–Visible Radiation. J Cluster Sci. 2021;33(6):2475-2487.
39. Kiani A, Nabiyouni G, Masoumi S, Ghanbari D. A novel magnetic $MgFe_2O_4$–$MgTiO_3$ perovskite nanocomposite: Rapid photo-degradation of toxic dyes under visible irradiation. Composites Part B: Engineering. 2019;175:107080.
40. Alomairy S, Gnanasekaran L, Rajendran S, Alsanie WF. Nanosized core-shell ($NiFe_2O_4/TiO_2$) heterostructure for enhanced photodegradation against polycyclic aromatic hydrocarbons. Chemosphere. 2023;343:140274.